Proceedings of the 28th IEEE
EMBS Annual International Conference
New York City, USA, Aug 30-Sept 3, 2006

Non-invasive Diagnosing Malignant Melanoma by Multi-spectral Optical Nevoscope

Song Wang, B.S., Atam P. Dhawan, Ph.D., IEEE Fellow

Abstract—**Malignant melanoma is one of the most fatal forms of skin cancer. There are two significant signs indicating malignancy of a melanoma, that is, abnormal melanin distribution in dermis layer and a peripheral blood net. We developed a multi-spectral optical Nevoscope aimed to diagnosing malignant melanoma non-invasively. An algorithm is proposed to reconstruct the melanoma in terms of Nevoscope geometry. The algorithm has been verified on an optical tumor model at 580nm and 800nm. The reconstructed melanoma is consistent with the tumor model which suggests a great potential of using Nevoscope to investigate malignant melanoma.**

I. Introduction

A recent report shows that skin cancer is one of fastest growing cancer among all cancers [1]. Malignant melanoma, the most fatal skin cancer, is fatal if not detected and removed at its early stage. There are two significant signs indicating malignancy of a melanoma. First, melanin usually presents in the epidermis layer of healthy skin. When it is a malignant melanoma, melanin also appears in the deeper layers such as dermis due to uncontrolled duplication of cancer cell. Second, to grasp sufficient nutrient to support its growth, malignant melanoma usually has a peripheral blood net. These changes in melanin and blood distribution also lead to varied appearance of malignant melanoma. So physicians usually use the "ABCD" rule to determine if the lesion under examination is malignant. The "ABCD" refers to asymmetry, border, color and diameter respectively. However, diagnosis accuracy by the "ABCD" rule is no better than 50%.

Non-invasive medical imaging modalities have been widely used nowadays. Nonetheless, there are still limitations in these well-established modalities. In particular, since these modalities are designed with different physical principles, the reconstructed image only stands for physical properties with respect to a specific source. So they only tell part of the whole story. Until now, there have few non-invasive modalities that can examine malignant melanoma effectively and reliably. Multi-spectral optical Nevoscope is a modality introduced by Dhawan [2] aimed to diagnosing malignant melanoma non-invasively. Its trans-illumination image is formed by backscattered diffused light that re-emerges from skin (Fig.1). Through the process of trans-illumination, the resultant image carries information about the sub-surface structures of skin and skin-lesion. It can therefore be utilized to reconstruct inner structures. Due to the differed absorption spectra of blood and melanin, reconstructions at multiple wavelengths can be used to reveal spatial distributions of blood and melanin and consequently indicate malignancy of melanoma.

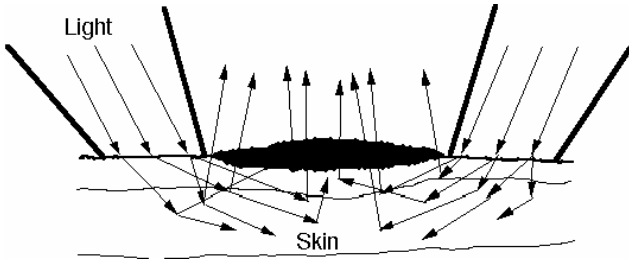

Fig.1. Trans-illumination mode of Nevoscope

II. Method

Regardless of the arrangement of light source and detector, the forward process of an optical tomographic system may be expressed as

$$\vec{m} = F(\vec{x}) \quad (1)$$

Where $\vec{m}$ is the measurement and $\vec{x}$ is unknown optical properties. F is a forward model.

Theoretically, photon transportation in tissue can be adequately modeled as radioactive transport equation (RTE) [3]. However, from a computation standpoint it is a formidable task to solve the equation directly. Instead, Diffuse Approximation (DA) and Monte Carlo simulation (MC) [4] are often used. When scattering is a more dominant phenomenon than absorption, direction dependent radiance can be well approximated as isotropic fluence rate and RTE may be simplified to DA. As a relative fast forward model, DA is extensively adopted in the literature. Unfortunately, to make the model valid, scattering coefficient must be much greater than absorption coefficient [5]. As to malignant melanoma, melanin is a high absorption chromophore over the whole visible and near-infrared spectra. The validity of DA under this scenario is questionable. So the statistical Monte Carlo simulation is adopted as the forward model in our study.

Once there is an agreement on the forward model, we may formulate the inverse problem as

$$\vec{x} = F^{-1}(\vec{m}) \quad (2)$$

Where F^{-1} is an inverse operator.

Manuscript received April 3, 2006.

Atam P. Dhawan is with the department of Electrical and Computer Engineering, New Jersey Institute of Technology, Newark, NJ 07032 USA. (phone: 973-596-5442; email: atam.p.dhawan@njit.edu)

Song Wang is with the Department of Electrical and Computer Engineering, New Jersey Institute of Technology, Newark, NJ 07032 USA. (email: sw29@njit.edu).

The inverse problem may be formulated as a linear system relating local perturbation to the changes in measurement or as a non-linear optimization problem to minimize the difference between model prediction and real measurement.

The Taylor expansion of (1) results

$$\vec{m} = F(\vec{x}_0) + F'(\vec{x}_0)(\vec{x} - \vec{x}_0) + \frac{1}{2}F''(\vec{x}_0)(\vec{x} - \vec{x}_0)^2 + \ldots \quad (3)$$

Here, x_0 is some known background. F' and F'' are the first order and second order derivative of the forward model respectively. If neglecting the second and higher order derivatives, (3) leads to a linear formulation of the inverse problem

$$\vec{x} = (F'(\vec{x}_0))^{-1}(\vec{m} - F(\vec{x}_0)) + \vec{x}_0 \quad (4)$$

It is also known as "difference imaging". That is, two images are fed to (4). One is the image from a background with known optical properties and the other is the image from the medium with the object of interest imbedded in the background.

The inverse problem could also be set up to minimize an object function

$$O(\vec{x}) = \left\| \vec{m} - F(\vec{x}) \right\|^2 \quad (5)$$

Alternative formulations of (5) may include some terms to further constrain the solution. For simplicity purpose, most algorithms only use the gradient of the object function. They usually involve iterative linear steps. Each step is similar to (4) and the corresponding F' has to be updated.

For a non-linear approach, F' has to be re-evaluated at each step. Unfortunately, MC is not fast enough to afford that. The linear formulation (4) is therefore adopted in our application.

In the following subsections, the optical properties of skin, the forward model and the inverse strategy are discussed in detail.

A. Optical Properties of Skin

The anatomical structure of skin shows that it has several layers with distinct characteristics. We adopted a seven-layered skin model which is consistent with histological study [6].The skin model is divided into seven layers in terms of concentration of major absorbers and microscopic structure of skin. They are stratum corneum ($20\,\mu m$), epidermis ($80\,\mu m$), dermis ($150\,\mu m$), upper blood net dermis ($80\,\mu m$), reticular dermis ($1500\,\mu m$), deep blood net dermis ($100\,\mu m$) and subcutaneous fat ($6000\,\mu m$). The thicknesses given above are typical values for most part of human body.

The absorption coefficient of each layer is a combined effect contributed by several absorbers such as Oxy-hemoglobin, deOxy-hemoglobin, melanin, water and baseline skin which is free of aforementioned absorbers. The absorption coefficient of baseline skin is given by Jacques [7] as

$$\mu_a^{\,baseline}(\lambda) = 7.84 \times 10^8 \times \lambda^{-3.255} (cm^{-1}) \quad (6)$$

Here, λ is the wavelength measured in nanometer.

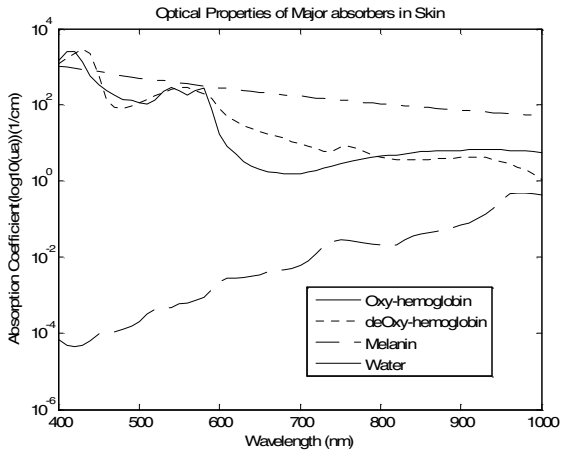

Fig. 2. Optical properties of major absorbers in Skin

The absorption coefficient of melanin is given as [6]

$$\mu_a^{\,melanin}(\lambda) = 5 \times 10^{10} \times \lambda^{-3.33} (cm^{-1}) \quad (7)$$

The absorption coefficients of water, Oxy-hemoglobin and deOxy-hemoglobin (Fig. 2) come from Jacques [7].

Absorption coefficients of two blood free layers stratum corneum and epidermis are predicted by (8) and (9)

$$\mu_a^{\,stratum}(\lambda) = ((0.1 - 0.3 \times 10^{-4}\lambda) + 0.125\mu_a^{\,baseline}(\lambda))(1 - C_{H_2O}) + C_{H_2O}\mu_a^{\,H_2O}(\lambda) \quad (8)$$

$$\mu_a^{\,epi}(\lambda) = C_{melanin}\mu_a^{\,melanin}(\lambda) + C_{H_2O}\mu_a^{\,H_2O}(\lambda) + (1 - C_{melanin} - C_{H_2O})\mu_a^{\,baseline}(\lambda)) \quad (9)$$

In the above equations, $C_{melanin}$ is the fraction of melanin in epidermis and C_{H_2O} is the fraction of water in a specific layer.

Absorption coefficients of four dermis layers and subcutaneous fat are described by one formula (10) while their values depend on how much blood and water they contain.

$$\mu_a^{\,bloodlayer}(\lambda) = C_{blood}\mu_a^{\,blood}(\lambda) + C_{H_2O}\mu_a^{\,H_2O} + (1 - C_{blood} - C_{H_2O})\mu_a^{\,baseline} \quad (10)$$

Here, C_{blood} is the fraction of blood presented in a layer.

Light scattering in skin is determined by Mie scattering and Rayleigh Limit scattering [7]. The former delineates scattering by relatively large structure such as dermal collagen fibers and epidermal keratin fibers while the latter explains scattering by small cellular structures. As to skin, Mie scattering is a dominant phenomenon. We therefore assume skin scattering is independent of variations of major absorbers. The anisotropy factor ranges from 0.7 to 0.9 for biological medium, which means a strong forward scattering. Representative values of optical properties and fractions of absorbers are compiled by Igor [6].

B. Forward Modeling

MC simulations are widely used for optical modeling imaging [8-11]. A Monte Carlo code is also developed by our group to model the forward photon transportation for Nevoscope. It first records photon paths reaching specific

detectors. The received intensities are then calculated according to the optical properties of the interrogated medium. The procedure is described below.

First, a photon is launched to simulate a ring light. It location is defined as

$$\begin{cases} x_0 = r\cos(2\pi\xi) \\ y_0 = r\sin(2\pi\xi) \end{cases} \tag{11}$$

Where ξ is a uniform random number between 0 and 1.

Because of the discrepancy of refractive indices between air and skin, the photon will change its incident direction according to Snell's law. And the photon loses part of its energy due to specular reflection. Assuming each photon has normalized energy 1, the remaining energy is given by

$$w_0 = 1 - \frac{1}{2}\left[\frac{\sin^2(\alpha_i - \alpha_t)}{\sin^2(\alpha_i + \alpha_t)} + \frac{\tan^2(\alpha_i - \alpha_t)}{\tan^2(\alpha_i + \alpha_t)}\right] \tag{12}$$

In (12), $\alpha_i = 45^0$ is the incident angle and α_t is the transmitted angle.

After the photon is launched, it undergoes multi-scattering events until it hits the detector. The path length between scattering events is given as

$$l = -\frac{\ln(\xi)}{\mu_s} \tag{13}$$

At each scattering point, the photon will change to a new direction. The direction is sampled from the Henyey and Greenstein phase function. Photon crossing internal boundaries is handled with the "Russian roulette" approach proposed by Wang etc. [11].

When the photon reaches a detector, it may hit the skin surface several times and lose part of its energy each time. Let us assume the photon hits the surface h times and $R(\alpha)$ stands for Fresnel reflection coefficient given the hitting angle α. The remaining weight becomes

$$w_d = (1 - R(\alpha_h))w_0 \sum_{i=1}^{h-1} R(\alpha_i) \tag{14}$$

The final weight received by the detector may be calculated in terms of microscopic Beer's law as

$$I = w_d \sum_{j=1}^{q} e^{-\mu_a(j)l_j} \tag{15}$$

Here we assume the photon takes q steps and $\mu_a(j)$ is the absorption coefficient along the path l_j.

A large number of photons should be launched to obtain a statistically meaningful result.

C. Inverse Strategy

In our study, two trans-illumination images are taken. One is from malignant melanoma. The other is from nearby normal skin and served as background. Now, let's divide the field of view of Nevoscope into M layers and each layer contains $N \times N$ voxels. And the detector plane is divided into T pixels. We may re-write (4) to a discrete form

$$\Delta\vec{I} = J\Delta\vec{\mu}_a \tag{16}$$

Where $\Delta\vec{I}$ is the difference in measurement and $\Delta\vec{\mu}_a$ is the change in absorption.

For the normal skin or the background medium, the received intensity by a detector is given as

$$I(s) = \sum_{i=1}^{p_s} w^i_{skin} = \sum_{i=1}^{p_s} \left({w_d}^i \sum_{j=1}^{N\times N\times M} e^{-\mu_a(j)l_j^i} \right) \tag{17}$$

Here, $s = 1,...T$. p_s is total number of photons received by the detector s. l_j^i is the path length of photon i in the voxel j. $\mu_a(j)$ is the absorption coefficient of voxel j corresponding to that of normal skin.

The variation in measurement may be expressed in terms of changes in local absorption as

$$\Delta I(s) = \sum_{i=1}^{p_s} \left({w_{skin}}^i \sum_{j=1}^{N\times N\times M} e^{-\Delta\mu_a(j)l_j^i} \right) \tag{18}$$

Taking the derivative with respect to $\Delta\mu_a(j)$ and set $\Delta\mu_a(j)$ to zero, we obtain

$$\left.\frac{\partial \Delta I(s)}{\partial \Delta\mu_a(j)}\right|_{\Delta\mu_a(j)=0} = \sum_{i=1}^{p_s} ({w_{skin}}^i \cdot l_j^i) \tag{19}$$

Now, the Jacobian matrix can be evaluated as

$$J = \left[\begin{array}{ccc} \frac{\partial \Delta I(1)}{\partial \Delta\mu_a(1)} & \frac{\partial \Delta I(1)}{\partial \Delta\mu_a(2)} & \frac{\partial \Delta I(1)}{\partial \Delta\mu_a(N\times N\times M)} \\ \cdot & \cdot & \cdot \\ \cdot & \cdot & \cdot \\ \cdot & \cdot & \cdot \\ \frac{\partial \Delta I(T)}{\partial \Delta\mu_a(1)} & \frac{\partial \Delta I(T)}{\partial \Delta\mu_a(2)} & \frac{\partial \Delta I(T)}{\partial \Delta\mu_a(N\times N\times M)} \end{array}\right]_{\Delta\mu_a(j)=0} \tag{20}$$

The solution of (16) gives spatial distribution of changes in absorption. However, usually the matrix (20) is an ill-conditioned one which means its direct inverse does not exist. Common approaches to solving (16) include Algebraic Reconstruction Technique (ART), Truncated Singular Value Decomposition (TSVD) and Conjugate Gradient method (GC). In our study, we found that ART has a smoother result but fails to resolve the depth of invasion. Both TSVD and GC offer reasonable results. These results agree with a comparison study by Gaudette [12]. Since GC is also a memory efficient algorithm compared to TSVD, it is finally adopted in our reconstruction algorithm.

III. RESULTS AND DISCUSSION

The proposed algorithm is verified for the Nevoscope with a 1.2*cm* diameter. Its 1.2*cm* diameter detector plane is divided into 20 rings with equivalent width. Each ring is further broken into a number of detectors and all detectors maintain the same size. The objective is to avoid error when their values are interpolated from trans-illumination image. In addition, when the Jocobian matrix is evaluated, only photon histories of one detector need to be recorded for each ring. Photon histories of other detectors at the same ring can be obtained by rotating the recorded ones. This greatly

reduces the storage space of photon histories and shorts the computation time. In our case, 1588 detectors are used finally. To evaluate Jacobian matrix, a $1.2\times1.2\times0.1cm^3$ field of view is divided into $32\times32\times10$ voxels. The matrix is calculated from skin optical properties introduced before.

Moreover, an optical tumor model is designed to evaluate the proposed algorithm (Fig.3.a&b). A tumor with the volume $0.375\times0.375\times0.04cm^3$ is embedded into normal skin model. Upper part of the tumor with volume $0.375\times0.375\times0.03cm^3$ is modeled as skin background added by 5% melanin, which simulates invasion of melanin in dermis. Lower part with volume $0.375\times0.375\times0.01cm^3$ is modeled as skin background added by 40% blood which simulates the peripheral blood net. The absorption of water is low over visible and near-infrared spectra, so it is not included in the model. Two images are generated using MC simulation on normal skin model and the tumor model respectively. Their difference is fed to the left hand side of (16).

The reconstructed results at 580nm and 800nm are shown in Fig. 3.c and Fig. 3.d respectively. Layers 1 to layer 10 are listed from left to right and from top to bottom. At these two wavelengths, deOxy-hemoglobin and Oxy-hemoglobin have identical absorption coefficients. So we don't need consider oxygen saturation of blood. The results have been re-scaled in terms of their maximum reconstructed values at 580nm and 800nm respectively. So the brighter regions correspond to higher absorption coefficients. In both results, high absorption can be observed from layer 2 to layer 4, which means these layers contain melanin. Additionally, high absorption is presented in layer 5 at 580nm while there is only low absorption in the same layer at 800nm. It means layer 5 must contain a blood net according to the absorption spectrum of blood. The results are consistent with the optical tumor model which suggests that multi-spectral optical Nevoscope has a great potential to be utilized to characterize malignant melanoma.

The final objective of this study is to present spatial distributions of melanin and blood through multi-spectral measurement. To achieve this, two problems would be addressed in our future study. First of all, the quality of reconstruction may be improved with optimally selected wavelengths. Sachin [13] has illustrated a linear correlation analysis to select wavelengths for Nevoscope. We are going to extend it to near-infrared spectra. In addition, as indicated by Corlu [14], wavelengths used in optical imaging also affect separation of choromophores. This will also be taken into our consideration. Secondly, it is well known that inverse problem of optical tomography is a typical under-determined one. Out of many possible solutions, the expected one should meet some prior hypothesis such as smoothness [15] or be constrained by prior information [16]. We believe incorporating such information would offer a more reliable result.

REFERENCES

[1] The skin cancer foundation (www.skincancer.org).

[2] Dhawan, A. P., R. Gordon, and R. M. Rangayyan, "Nevoscopy: three-dimensional computed tomography for nevi and melanoma by transillumination", IEEE Trans. on Medical Imaging, vol. MI-3(2), pp. 54-61, 1984.

[3] Chandrasekhar, R. *Radiation transfer*, Oxford: Clariendon Press. 1950.

[4] Arridge, S. R, Hebden.J, "Optical imaging in medicine II: modeling and reconstruction", Phys. Med. Biol. 42(5), 841, 1997.

[5] M. Firbank , S.R. Arridge, M. Schweiger and D.T. Delpy, "An investigation of light transport through scattering bodies with non-scattering regions", Phys. Med. Biol. 41, 767-783,1996.

[6] Igor. V. Meglinski and Stephen J Matcher, "Quantitative assessment of skin layers absorption and skin reflectance spectra simulation in the visible and near-infrared spectral regions, Physiol. Meas, 23, pp. 741-753, 2002.

[7] Steven L. Jacques, Oregon Medical Center News, Jan 1998.

[8] Angelo Sassaroli etc., "Monte Carlo procedure for investigating light propagation and imaging of highly scattering media", Appl. Opt., Vol. 37, No. 31, 1998.

[9] R. Graaff, M. H. Koelink, F. F. M. de Mul, W. G. Zijistra, A. C. M. Dassel, and J. G. Aarnoudse, Condensed Monte Carlo simulations for the description of light transport , Appl. Opt. Vol. 32, No. 4 ,1993.

[10] Johannes Swartling, Antonio Pifferi, Annika M. K. Enejder, Stefan Andersson-Engels, Accelerated Monte Carlo models to simulate fluorescence spectra from layered tissues , J. Opt. Soc. Am. Vol. 20, No. 4 2003.

[11] L. Wang, S. L. Jacques and L. Zheng, MCML-Monte Carlo modeling of light transport in multi-layered tissues, Computer Methods and Programs in Biomedicine 47, 131-146 (1995).

[12] Richard J G, Dana H B and Charles A Dimarzio, "A comparison study of linear reconstruction techniques for diffuse optical tomographic imaging of absorption coefficient", Phys. Med. Biol. 45, 1051-1070, 2000.

[13] Sachin V. Patwardhan, Atam P. Dhawan and Patricia A. Relue, "Wavelength selection for multi-spectral imaging of skin lesions using Nevoscope ", Proc. IEEE 29th Annual Northeast Bioengineering Conference,327-328, 2003

[14] Alper Corlu etc. "Diffuse optical tomography with spectral constraints and wavelength optimization", Appl. Opt.., Vol. 44, No. 11, 2005

[15] Wenwu Zhu, Yao Wang, Nikolas P. Galatsanos, and Jun Zhang, "Regularized Total Least Squares Approach for Nonconvolutional Linear Inverse Problems" , IEEE Trans. On Medical Imaging. Vol.8, No. 11, 1999

[16] Ang Li etc. "Optimal linear inverse solution with multiple priors in diffuse optical tomography", Appl. Opt., Vol. 44, No. 10,2005

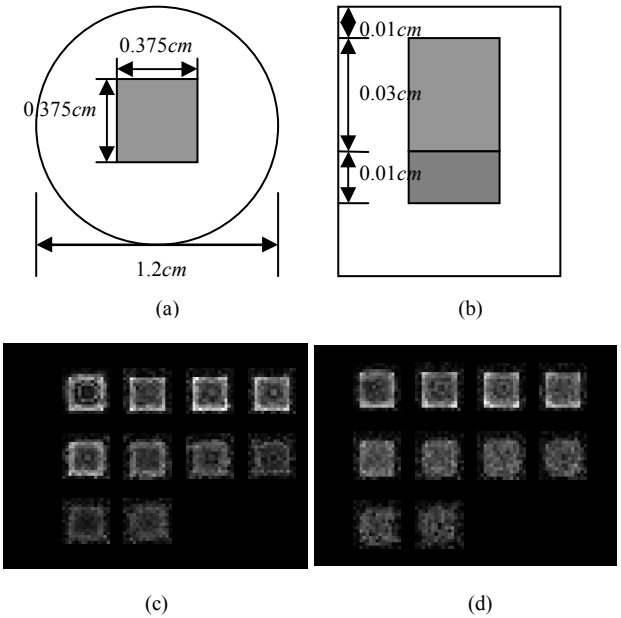

Fig. 3. (a) Tumor model at x-y plane. (b) Tumor model at x-z plane. (c) Reconstruction at 580nm. (d) Reconstruction at 800nm